Journal Pre-proof

Localized characterization of brain tissue mechanical properties by needle induced cavitation rheology and volume controlled cavity expansion

Aleksandar S. Mijailovic, Sualyneth Galarza, Shabnam Raayai-Ardakani, Nathan P. Birch, Jessica D. Schiffman, Alfred J. Crosby, Tal Cohen, Shelly R. Peyton, Krystyn J. Van Vliet

PII: S1751-6161(20)30710-4

DOI: https://doi.org/10.1016/j.jmbbm.2020.104168

Reference: JMBBM 104168

To appear in: *Journal of the Mechanical Behavior of Biomedical Materials*

Received Date: 7 February 2020

Revised Date: 10 August 2020

Accepted Date: 23 October 2020

Please cite this article as: Mijailovic, A.S., Galarza, S., Raayai-Ardakani, S., Birch, N.P., Schiffman, J.D., Crosby, A.J., Cohen, T., Peyton, S.R., Van Vliet, K.J., Localized characterization of brain tissue mechanical properties by needle induced cavitation rheology and volume controlled cavity expansion, *Journal of the Mechanical Behavior of Biomedical Materials* (2020), doi: https://doi.org/10.1016/j.jmbbm.2020.104168.

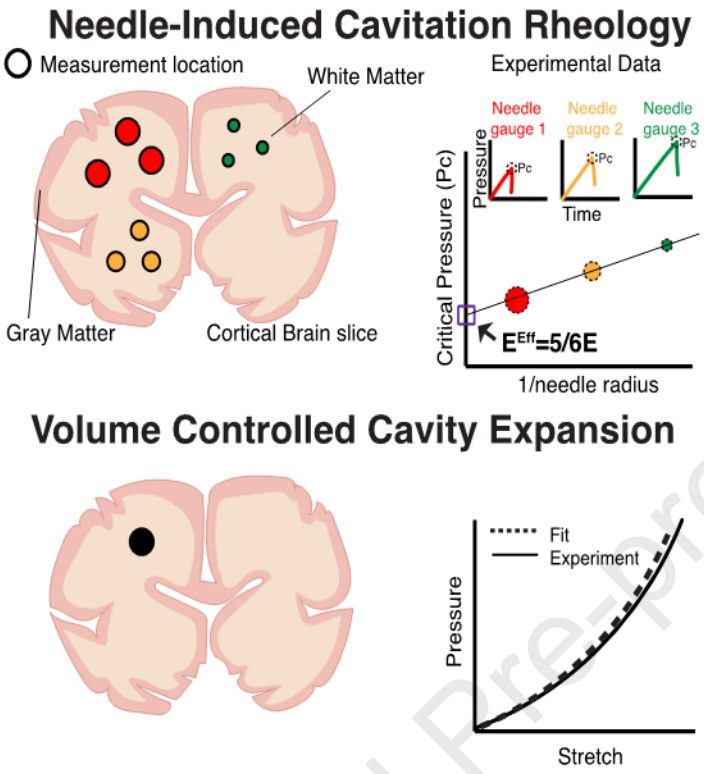

Journal Mechanical Behavior of Biomedical Materials

ARTICLE

Localized Characterization of Brain Tissue Mechanical Properties by Needle Induced Cavitation Rheology and Volume Controlled Cavity Expansion

Aleksandar S. Mijailovic[a, x], Sualyneth Galarza[b, x], Shabnam Raayai-Ardakani[c, x], Nathan P. Birch[b], Jessica D. Schiffman[b], Alfred J. Crosby[d], Tal Cohen[c], Shelly R. Peyton[b, *], Krystyn J. Van Vliet[e,f, *]

Cite this: DOI: xxxxx/x0xx00000x

Received 7th February 2020,
Accepted 00th XX 2020
DOI: xxxxx/x0xx00000x

[a] Department of Mechanical Engineering, Massachusetts Institute of Technology, Cambridge, MA 02139, USA
[b] Department of Chemical Engineering, University of Massachusetts-Amherst, Amherst, MA, 01003, USA
[c] Department of Civil and Environmental Engineering, Massachusetts Institute of Technology, Cambridge, MA 02139, USA
[d] Department of Polymer Science and Engineering, University of Massachusetts-Amherst, Amherst, MA, 01003, USA
[e] Department of Materials Science and Engineering, Massachusetts Institute of Technology, Cambridge, MA 02139, USA
[f] Department of Biological Engineering, Massachusetts Institute of Technology, Cambridge, MA 02139, USA
[x] These authors contributed equally.
[*] Corresponding authors
Departments of Materials Science and Engineering and Biological Engineering, Massachusetts Institute of Technology, 77 Massachusetts Ave, Cambridge, MA 02139, USA. E-mail address: krystyn@mit.edu (K.J. Van Vliet).

Abstract

Changes in the elastic properties of brain tissue have been correlated with injury, cancers, and neurodegenerative diseases. However, discrepancies in the reported elastic moduli of brain tissue are persistent, and spatial inhomogeneities complicate the interpretation of macroscale measurements such as rheology. Here we introduce needle induced cavitation rheology (NICR) and volume-controlled cavity expansion (VCCE) as facile methods to measure the apparent Young's modulus E of minimally manipulated brain tissue, at specific tissue locations and with sub-millimeter spatial resolution. For different porcine brain regions and sections analyzed by NICR, we found E to be 3.7 ± 0.7 kPa and 4.8 ± 1.0 kPa for gray matter, and white matter, respectively. For different porcine brain regions and sections analyzed by VCCE, we found E was 0.76 ± 0.02 kPa for gray matter and 0.92 ± 0.01 kPa for white matter. Measurements from VCCE were more similar to those obtained from macroscale shear rheology (0.75 ± 0.06 kPa) and from instrumented microindentation of white matter (0.97 ± 0.40 kPa) and gray matter (0.86 ± 0.20 kPa). We attributed the higher stiffness reported from NICR to that method's assumption of a cavitation instability due to a neo-Hookean constitutive response, which does not capture the strain-stiffening behavior of brain tissue under large strains, and therefore did not provide adequate measurements. We demonstrate via both analytical modeling of a spherical cavity and finite element modeling of a needle geometry, that this strain stiffening may prevent a cavitation instability. VCCE measurements take this stiffening behavior into account by employing an incompressible one-term Ogden model to find the nonlinear elastic properties of the tissue. Overall, VCCE afforded rapid and facile measurement of nonlinear mechanical properties of intact, healthy mammalian brain tissue, enabling quantitative comparison among brain tissue regions and also between species. Finally, accurate estimation of elastic properties for this strain stiffening tissue requires methods that include appropriate constitutive models of the brain tissue response, which here are represented by inclusion of the Ogden model in VCCE.

Journal to which we will submit

Journal logo

ARTICLE

Key words: biomechanics; indentation; shear rheology; Young's modulus; cavitation rheology; Ogden model

ARTICLE

1.Introduction

Changes in the elastic moduli and the rate-dependent properties of brain tissue have been reported to correlate with Alzheimer's disease, traumatic axonal injuries, cortical contusions and brain tumors (Boulet et al., 2011; Jamin et al., 2015; Murphy et al., 2011; Streitberger et al., 2011; Wuerfel et al., 2010). Animal models of traumatic brain injury (TBI) and cancer examined via magnetic resonance elastography (MRE) have also noted local reduction in apparent stiffness at the injured site following a local lesion (Boulet et al., 2011; Jamin et al., 2015). At the microscale, cells in the central nervous system (CNS) have been shown to respond phenotypically to mechanical cues and depending on local stiffness (Franze et al., 2013; Jagielska et al., 2012; Pogoda et al., 2014; Tyler, 2012; Wang et al., 2014). Those studies highlighted the importance of understanding mechanical properties of brain tissue, including spatial variations and changes with disease progression. Additionally, the design of *in vitro* systems that recapitulate key mechanical properties of healthy brain tissue are of interest for neurosurgical applications, tissue engineering, modeling of TBI, and the design of tissue simulant materials. However, there is no consensus on the magnitude of several key *in vivo* mechanical properties or the macroscale constitutive relation of this tissue (Budday et al., 2019).

Several studies approximate brain tissue as a linear elastic and isotropic solid, and thus summarized the tissue stiffness in terms of Young's modulus *E*. Reports of *E* of brain tissue range across several orders of magnitude (i.e. 100-10,000 Pa) (Cheng et al., 2008; Franze et al., 2013; Tyler, 2012), and vary considerably among experimental techniques (Chatelin et al., 2010; Cheng et al., 2008; Hrapko et al., 2008a). Moreover, the underlying assumptions of linear elastic deformation and homogeneous isotropic response are tenuous for this complex biological material under most experimental loading conditions. Many studies have demonstrated that brain tissue can exhibit considerable nonlinear strain-stiffening behavior under both compression and tension at sufficiently high strains that typically exceed 1-10% (Franceschini et al., 2006; Pogoda et al., 2014; Prevost et al., 2011; Rashid et al., 2012) although this has not been observed in all cases (Prange and Margulies, 2002). The strain-stiffening behavior at low deformation rates was often captured by fitting the hyperelastic components of hyper-viscoelastic models to the assumed "equilibrium" response. This tissue can exhibit viscoelastic (i.e, time- and rate-dependent) deformation and effective stiffness, as experiments using macroscale rheology, stress relaxation and creep compliance demonstrated explicitly (Hrapko et al., 2006; Nicolle et al., 2005; Prange and Margulies, 2002). However, the reported viscoelastic properties such as shear storage modulus *G'* and loss modulus *G"* also span orders of magnitude among various studies, and are characterized generally by weak power laws (Chatelin et al., 2010; Hrapko et al., 2008a). As each experimental technique includes limitations of deformation modes and magnitudes, particularly for materials as structurally and mechanically complex and compliant as brain tissue (Canovic et al. 2016), prior work has established that magnitudes of these reported values can also vary with experimental technique (Budday et. al. 2019, Canovic et al. 2016). Additionally, brain tissue exhibits strain rate dependent behavior even at timescales on the order of 100s to 1000s of seconds, so characterizing the actual "equilibrium" behavior via fits to viscoelastic or hyper-viscoelastic models is elusive even under deformation rates that would be considered quasistatic for practical uses (Chatelin et al., 2010; Hrapko et al., 2008a). Therefore, reports of "equilibrium moduli" for brain tissue must be interpreted with caution. Further, the stiffness of brain tissue is strain-history dependent, as preconditioning of the tissue has been known to reduce the stiffness as compared to virgin tissue (Franceschini et al. 2006, Budday et al. 2017, Budday et al. 2019). Nevertheless, modeling the "equilibrium" behavior with hyperelastic models under low strain rate conditions without considering rate dependent behavior has proven useful in recent studies (Mihai et al 2015, Mihai et al., 2017). Finally, under very specific deformation rates and length scales, brain tissue can exhibit poroelastic responses at the macroscale, as has been demonstrated by unconfined uniaxial compression or tension (Budday et al., 2017; Cheng and Bilston, 2007; Franceschini et al., 2006; Miller and Chinzei, 2002).

While macroscale mechanical properties may be relevant for some applications including modeling of head protection strategies, for many applications the mechanical heterogeneity of brain tissue is an important feature to capture. Brain tissue includes regions that differ visibly in the extent of neuron myelination and are referred to as white matter (higher myelin content) or gray matter (less myelin). Some studies have reported white matter to be stiffer than gray matter (Budday et al., 2015; Prange and Margulies, 2002; van Dommelen et al., 2010; Velardi et al., 2006), while other studies have concluded that gray matter is stiffer than white matter (Budday et al., 2017; Green et al., 2008). Even still other studies have noted the presence of local variations in stiffness within white matter (Chen et al., 2015; Prange and Margulies, 2002), and that white matter is elastically anisotropic (Franceschini et al., 2006; Hrapko et al., 2008b; Prange and Margulies, 2002; van Dommelen et al., 2010). Microscale experiments such as instrumented indentation (Budday et al., 2015; Chen et al., 2015; Gefen and Margulies, 2004; Miller et al., 2000;

van Dommelen et al., 2010), atomic force microscopy-enabled indentation (Canovic et al., 2016; Elkin and Morrison, 2013; Urbanski et al., 2019) and magnetic resonance elastography (Murphy et al., 2011) have helped to explore such local differences. However, these spatially resolved approaches are still limited by highly constrained assumptions of tissue constitutive behavior, and deformation volumes that are convoluted by the probe geometry and tissue heterogeneity. Taken together, prior studies also indicate that the mechanical properties of brain tissue – even when idealized by simple constitutive models or identified as white or gray matter – vary across anatomical regions within the organ (Chen et al., 2015; Elkin et al., 2011; Lee et al., 2014; Pogoda et al., 2014; Prange and Margulies, 2002; van Dommelen et al., 2010).

To address current limitations in accurate and spatially localized measurement of brain tissue constitutive response, we introduce two related and distinct cavitation-based methods to quantify (hyper)elastic properties of brain tissue regions. Both approaches deliver pressurized fluid through a narrow needle to deform the tissue locally. Needle induced cavitation rheology (NICR) has been used previously to measure elastic and fracture properties of polymers, as well as eye lens *ex vivo*, bone marrow tissue *in situ* and skin *in vivo* (Chin et al., 2013; Cui et al., 2011; Jansen et al., 2015; Kundu and Crosby, 2009; Zimberlin et al., 2010; Zimberlin et al., 2007). This technique requires a cavitation instability to occur within the material and be detectable at a finite applied fluid pressure; application of a constitutive law such as the hyperelastic neo-Hookean model affords estimates of E on the length scale of micrometers to millimeters. This approach has been validated by finite element (FE) simulations and macroscale rheology (Hutchens and Crosby, 2014; Hutchens et al., 2016; Jansen et al., 2015; Kundu and Crosby, 2009; Zimberlin et al., 2010). Volume controlled cavity expansion (VCCE) has been used to measure nonlinear elastic properties of compliant polymers. Since VCCE is an extension of NICR methodology, VCCE has the same capabilities of *in situ*, localized measurements as NICR. However, since VCCE also allows measurement of both pressure and volume of the injected incompressible fluid, cavitation events are not required and any incompressible hyperelastic constitutive equation can be fit to the resulting data. Mechanical properties can be obtained from a single VCCE measurement, whereas determination of E with NICR can require multiple experiments with multiple needle diameters to account for surface tension effects. VCCE has been initially employed with a neo-Hookean model (Raayai-Ardakani et al., 2019a; Raayai-Ardakani et al., 2019b), and later extended to fracture events (Raayai-Ardakani et al., 2019b) and to account for strain stiffening (Raayai-Ardakani and Cohen, 2019). Here we expand the use of this technique to characterize hyperelastic behavior of the brain tissue with an incompressible one-term Ogden model that captures the strain-stiffening response (Franceschini et al., 2006; Mihai et al., 2017; Nicolle et al., 2004).

In this study, we evaluated NICR and VCCE as alternative, facile, approaches to characterize spatially localized apparent Young's modulus and nonlinear properties of brain tissue under "quasistatic" loading over time scales on the order of 10s to 100s of seconds. We conducted experiments in porcine brain, and validated those results against macroscale rheometry and microscale instrumented indentation. Because all experimental methods including these have inherent limitations and constrained choices, direct and quantitative comparison of extracted parameters among mechanical testing methods is challenging for materials such as brain tissue (Canovic et al., 2016; Budday et al., 2019). We thus qualify the measured parameter discussed herein as an *apparent* Young's modulus. Importantly, the limitations of each method and data analysis approach should be understood by the researcher, and are described here or elsewhere from practical and theoretical perspectives (Canovic et al., 2016; Budday et al., 2019; Raayai-Ardakani et al., 2019a; Raayai-Ardakani et al., 2019b). We demonstrate advantages of NICR and VCCE relative to those other characterization approaches, and verify that analytical models used to infer elastic properties are reasonably well approximated against finite element models with more accurate geometric representation of the pressurized needle inserted into a hyperelastic material.

2. Materials and Methods

2.1 Sample preparation

We obtained porcine brains from 6-12-month old pigs from Baystate Medical Center, Springfield MA, and Den Besten farm, Bridgewater, MA USA. We dissected porcine brains two hours post-mortem as four mm-thick coronal and transverse slices; we preserved these slices at 4^{o}C in phosphate-buffered saline (pH 7.4) or Hibernate-A media (pH 7) prior to testing.

ARTICLE

We conducted instrumented indentation on transverse sections, and we conducted VCCE and NICR on coronal or transverse sections. For rheometry, we obtained tissue samples by biopsy punch extraction for murine brain (8 mm wide and 1 mm thick), and by biopsy punch (8 mm diameter and 1 mm thick) or manual sectioning (25 mm diameter and 4 mm thick) for porcine brain. Tissue dehydration was minimized by placing all samples in ice-cold phosphate-buffered saline (pH 7.4) or Hibernate-A media (pH 7) and kept refrigerated at 4°C until mechanical testing. We conducted most experiments within 6 hours post mortem (Chatelin et al., 2010) to assure tissue integrity, and conducted all tests within 30 hours post mortem.

We obtained murine brains from B6 albino mice, 12 weeks old, from the Tremblay Lab at the University of Massachusetts Amherst, Amherst, MA USA. Murine brains were kept whole for indentation and NICR and tested 30 min post-mortem. Data from murine samples are provided in Supplementary Materials S1.

2.2 Theory and material models

The analytical models used to calculate Young's modulus *E* from NICR and VCCE experiments are based on analytical solutions of a pressurized spherical cavity in an infinitely large elastic medium. Specifically, the expansion of a spherically symmetric cavity in an elastic material under internal pressure *P* has been studied extensively for various material models (Horgan and Polignone, 1995). For the expansion of a cavity in an incompressible material, the principal stretches $\lambda_1, \lambda_2, \lambda_3$ may be expressed as $\lambda_2 = \lambda_3 = \lambda_\theta$ and $\lambda_1 = \lambda_\theta^{-2}$ where λ_θ is the circumferential stretch in the bulk material encapsulating the cavity (Horgan and Polignone, 1995). Here, circumferential stretch is defined as $\lambda_\theta = r/R_0$ where r is the deformed coordinate, and R_0 is the undeformed coordinate, and relates to engineering hoop strain ε_θ as $\lambda_\theta = 1 + \varepsilon_\theta$. For an isotropic, incompressible, hyperelastic material with a strain energy density function $W(\lambda_1, \lambda_2, \lambda_3)$, by defining $\widehat{W}(\lambda_\theta) = W(\lambda_\theta^{-2}, \lambda_\theta, \lambda_\theta)$, the relationship between *P* and the circumferential stretch at the cavity wall λ may be found with

$$P(\lambda) = \int_1^{\lambda} \frac{\widehat{W}'(\lambda_\theta)}{\lambda_\theta^3 - 1}\, \mathrm{d}\lambda_\theta\,, \tag{1}$$

where $\widehat{W}'(\lambda_\theta) = \frac{d\widehat{W}(\lambda_\theta)}{d\lambda_\theta}$, and it is assumed that the cavity is much smaller than the surrounding material. Further, the cavitation pressure (i.e, critical pressure P_c) can be found by integrating to infinite stretch at the cavity wall

$$P_c = \int_1^{\infty} \frac{\widehat{W}'(\lambda_\theta)}{\lambda_\theta^3 - 1}\, \mathrm{d}\lambda_\theta, \tag{2}$$

provided that the integral is convergent. Many studies characterizing tissues by NICR have assumed a neo-Hookean elastic constitutive law, which is defined by a strain energy density function

$$W_{NH} = \frac{E}{6}(\lambda_1^2 + \lambda_2^2 + \lambda_3^2 - 3). \tag{3}$$

From Eqs. (**1**) and (**3**), the pressure varies with stretch as

$$\frac{P}{E} = \frac{5}{6} - \frac{2}{3\lambda} - \frac{1}{6\lambda^4} \tag{4}$$

and combining Eq. (**2**) and (**3**), the critical pressure at which cavitation will occur is

$$P_c = \tfrac{5}{6}E. \tag{5}$$

Since brain tissue has been identified previously (Budday et al., 2017; Franceschini et al., 2006) as a strain-stiffening material, here we adopt a constitutive law that represents that behavior. Specifically, we employ an incompressible, *N*-term Ogden model with the strain energy density defined as

ARTICLE

$$W_{OG} = \sum_{i=1}^{N} \frac{2E_i}{3\alpha_i^2}(\lambda_1^{\alpha_i} + \lambda_2^{\alpha_i} + \lambda_3^{\alpha_i} - 3) \tag{6}$$

where α_i are constants that can reflect the strain-stiffening response of the material for $|\alpha_i| >> 2$ and $E = \sum_{i=1}^{N} E_i$. From Eqs. (**1**) and (**6**), the pressure-stretch relationship is

$$P = \sum_{i=1}^{N} \frac{4E_i}{3\alpha_i} \int_1^{\lambda} \frac{(\lambda_\theta^{3\alpha_i} - 1)}{(\lambda_\theta^3 - 1)} \frac{d\lambda_\theta}{\lambda_\theta^{2\alpha_i+1}}, \tag{7}$$

and the critical pressure for cavitation, if it exists, can be obtained from combining Eqs. (**2**) and (**6**), from which we get

$$P_c = \sum_{i=1}^{N} \frac{4E_i}{3\alpha_i} \int_1^{\infty} \frac{(\lambda_\theta^{3\alpha_i} - 1)}{(\lambda_\theta^3 - 1)} \frac{d\lambda_\theta}{\lambda_\theta^{2\alpha_i+1}}. \tag{8}$$

However, for P_c to be finite (i.e., for a cavitation instability to occur in the Ogden solid), each integral in the sum must be convergent. Elastic cavitation instability occurs provided that each exponent α_i is within the range (Chou-Wang and Horgan, 1989)

$$-\frac{3}{2} < \alpha_i < 3. \tag{9}$$

We note that these pressure-stretch relationships assume purely hyperelastic behavior and neglect the potential influence of surface tension, or of the potential viscoelasticity, poroelasticity, plasticity, damage and fracture of the material.

2.3 Needle Induced Cavitation Rheology (NICR)

Details of NICR have been described previously (Zimberlin et al., 2007). Briefly, a needle is embedded in a compliant solid, followed by pressurization of the fluid within the needle; this leads to the growth and rapid, unstable, expansion of a fluid-filled bubble at the tip of the needle. Our custom-built instrument consists of a syringe pump (New Era Syringe Pump NE1000 or Harvard Apparatus PHD Ultra), a pressure sensor (Omega Engineering PX26-001GV or Omega Engineering PX26-005DV), and a syringe needle connected to a DAQ card (National Instruments) that records the pressure as a function of time. Here, we inserted the needle into porcine (2.5 mm depth) and murine (1.8 mm depth) tissue samples and our working fluid of injection was air. Air injection velocity was 400 μL/min (which approximately corresponds to 1.8 kPa/min). We acquired measurements on white matter or gray matter tissue regions for porcine and murine cortex for a range of needle diameters or gauges (22-32 gauge, 0.413-0.108 mm inner diameter). We recorded pressure with a custom-developed LabVIEW code until a critical pressure P_c was reached. At the P_c, an instability arises, and the bubble rapidly expands while the pressure rapidly decreases with time. Assuming that the material is an isotropic, homogenous, neo-Hookean material, the apparent Young's modulus E was estimated using a modified form of Eq. (**5**) that also incorporates finite surface tension (Zimberlin et al., 2007)

$$P_c = \frac{5}{6}E + \frac{2\gamma}{R} \tag{10}$$

where R is the needle radius and γ is the surface tension. This result was obtained previously from analytical solutions of the elastic stress of a pressurized spherical void in an infinite solid and the surface tension of a spherical cap (Gent, 2005; Kundu and Crosby, 2009; Zimberlin et al., 2007). We thus obtained E for porcine and murine brain

tissue from Eq. (**10**) at 19-22^{o}C, fit to data obtained over a range of needle gauges and therefore a range of critical pressures which we assumed to be due to cavitation. We note that in this technique the deformation was assumed, and deformation rates could not be measured (or controlled for) as the cavity size could not be measured directly in the highly scattering media of this biological tissue.

2.4 Volume Controlled Cavity Expansion (VCCE)

VCCE has been discussed previously in detail by Raayai-Ardakani et al.(Raayai-Ardakani et al., 2019a; Raayai-Ardakani and Cohen, 2019). Briefly, this approach utilizes an incompressible working fluid and quantifies pressure while monitoring and controlling the injected fluid volume. Using a needle-syringe system connected to an Instron Universal Testing Machine, we expanded a cavity filled with incompressible liquid (here, silicone oil, which is immiscible in tissue) in a volume controlled manner at a rate of $2.7\ \mu L/s$ inside the material of interest. Needle diameters or gauges (gauge 22, 0.413 mm inner diameter) were chosen to minimize surface tension effects. Throughout the experiment, we monitored the pressure inside the cavity using a load cell connected to the syringe-piston, calibrated as discussed previously (Raayai-Ardakani et al., 2019a). We transformed the volume measurements at every instance of the experiment into an effective cavity radius a, and then fit the pressure-effective radius relationship to a one term Ogden model (see Eq. (**7**)) to obtain the elastic properties of the material (Raayai-Ardakani et al., 2019a; Raayai-Ardakani and Cohen, 2019). The fitting procedure and algorithms used herein are described in (Raayai-Ardakani and Cohen, 2019). Since, the initial cavity radius (a_0) is unknown we consider it as an additional unknown in the problem and fit *P*-λ for the three unknowns (i.e., *E*, α and a_0). The fitted initial cavity radius values are summarized in Supplementary Materials section S2, Table S1.

We characterized three porcine brains via VCCE at 19-22^{o}C. Due to the localized deformation of this experiment, we tested multiple distinct locations on each brain section; details are discussed in Supplementary Materials section S2. The stretch at the cavity wall λ was defined as $\lambda = (V/V_0)^{1/3}$. We note that the strain rate, while not constant throughout the deformed material due to the non-uniform strain field, can be approximated as an effective strain rate as $\dot{\varepsilon}_{\text{eff}} \approx \dot{\lambda}$. Since the rate of volumetric expansion was controlled in these experiments, the effective strain rate during deformation was not constant (see Eq. 15).

2.5 Indentation

We conducted instrumented indentation with a cylindrical flat punch (High-Speed M2 Tool Steel Hardened Undersized Rod, 1 or 1.5 mm diameter) at a fixed displacement rate (20 μm/s) and a maximum load (1.5 mN or 2 mN) in displacement control. A force transducer (Honeywell Sensotec, Columbus, OH) monitored the resulting load, F, while a nanoposition manipulator (Burleigh Instruments Inchworm Model IW-820) controlled the displacement δ. A material compliance factor *C*, calculated as the ratio between change in displacement over change in force,

$$C = \frac{d\delta}{dF} \tag{11}$$

was recorded by a National Instruments LabVIEW code. For the case of a contact radius much smaller than the dimensions of the elastic sample b with a correction confinement described by $0.5 < b/h < 2$ where h is the sample height, the effective apparent Young's modulus *E* can be calculated as (Shull et al., 1998):

$$E = \frac{3}{8C\left\{1 + 1.33\left(\frac{b}{h}\right) + 1.33\left(\frac{b}{h}\right)^3\right\}b} \tag{12}$$

We conducted indentation experiments on six porcine brains (transverse sections) at 19 to 22^{o}C. We also analyzed nine murine brains by this approach; see Supplementary Materials section S1.

ARTICLE

2.6 Rheology

We conducted small-amplitude oscillatory shear experiments on porcine (and murine; see Supplementary Materials section S1) brain slices using a Kinexus Pro rheometer (Malvern Instruments, UK) or an MCR 501 Rheometer (Anton Paar, Graz, Austria). The testing configuration was a parallel-plate geometry, with a sample diameter of 8 mm or 25 mm (and gap of 1 mm or 4 mm, respectively), at 25°C with oscillatory frequency sweeps between 0.1 and 1 Hz and under 0.5% or 1% shear strain. These strains were in the linear viscoelastic range as confirmed by amplitude sweep. The tissue was hydrated with either Hibernate-A media or deionized water. Finally, we approximated the apparent shear modulus G as the shear storage modulus G' at 0.1 Hz, and then related G to the apparent Young's modulus E assuming isotropic material behavior with a Poisson's ratio ν of 0.5:

$$E = 2G(1+\nu) = 3G. \tag{13}$$

We tested a total of nine porcine brains at 25°C.

2.7 Finite element modeling of VCCE and NICR

To assess the assumptions implicit in analysis of pressurized cavity deformation via NICR and VCCE, we modeled the deformation using a spherically symmetric analytical model (as described for NICR in section 2.2 and VCCE in section 2.3), as well as with finite element simulations of a needle-induced pressurization geometry. As in section 2.3, we expressed the load-deformation relationship in terms of applied pressure P and the circumferential stretch at the cavity wall λ. For the neo-Hookean constitutive model used to describe the spherically symmetric brain tissue deformation, we adopted Eq. (**4**). For the incompressible Ogden model, we used a two-term model (i.e., $N = 2$ in Eq. (**7**)), as was used previously in modeling brain tissue (Franceschini et al., 2006; Hutchens and Crosby, 2014)

To better approximate the experimental conditions of a pressurized needle in a large, compliant, and hyperelastic material, we created a 2D axisymmetric finite element model (ABAQUS software, Dassault Systemes, Providence, RI USA) of a thin-walled needle of radius R pressurizing a material volume of width at least 50 times greater than R. We considered two geometries: The first model included a needle that was inserted into the material, then retracted by a distance of one needle radius, such that a cylindrical cavity was formed; and the second included a needle that was inserted but not retracted. Figure S3b provides schematics of the geometry and boundary conditions. The second geometry is identical to that of Hutchens and Crosby (which predicted cavitation in brain in a finite element simulation of NICR), and also matches the boundary conditions and material models assumed in that work (Hutchens and Crosby, 2014). In both models used in the present work, the material was unstressed in the undeformed configuration, thus neglecting potential pre-stress prior to pressurization. We selected CAX3H linear, axisymmetric triangular elements and refined the mesh near the needle entrance. Pressure was applied on the free surface of the initial cavity or the material surface facing the needle opening, while no-displacement boundary conditions were enforced on the needle wall-material interface. We used two material models in our finite element analysis, the compressible Ogden model and the compressible neo-Hookean model, setting the Poisson's ratio to $\nu = 0.48$ to approximate the incompressible material behavior assumed in our spherically symmetric model. This value was chosen because higher Poisson's ratio values failed to converge at high stretch, and as previously confirmed by Hutchens and Crosby, ν had little effect on the pressure vs. stretch response in deformations relevant to NICR and VCCE (i.e., $\lambda_{\text{eff}} < 2$). Details of these material models and choice of Poisson's ratio are discussed in Supplementary Materials sections S3 and S4, respectively. We calculated the deformed cavity volume V as a function of normalized pressure P/E. Since the circumferential stretch at the cavity wall is a function of position, the effective cavity stretch λ_{eff} is then

$$\lambda_{\text{eff}} = \left(\frac{V}{V_0}\right)^{1/3} \tag{14}$$

where V_0 is the undeformed cavity volume. This differs from the method of Hutchens and Crosby that calculated areal stretch (Hutchens and Crosby, 2014) and reflects the volumetric stretch considered in VCCE. Nonetheless, it is of similar magnitude to the areal stretch calculation (see Supplementary Materials section S4).

For both the NICR and VCCE analysis, we included surface tension effects using the relations noted in Hutchens and Crosby for the Laplace pressure P_{Laplace} vs. stretch relationship of a deformed spherical cap:

$$P_{\text{Laplace}} \approx \frac{4\gamma}{R\lambda_{\text{eff}}^2}\sqrt{\lambda_{\text{eff}}^2 - 1} \quad (15)$$

We chose the surface tension of water ($\gamma = 72$ mN/m) due to a high water content of the tissue. We note that this is only an approximation of the surface tension response. We assumed that the total pressure was a sum of the pressure due to the elastic and surface tension responses. Also, since the undeformed state was assumed to be stress free, we also assumed that the surface tension effect did not lead to elastic stresses in the elastic body (in low radius of curvature areas) prior to pressurization.

2.8 Statistical Analysis

Statistical analysis was conducted with MATLAB software (Mathworks, Natick, MA). Statistical significance was evaluated using a one-way analysis of variance (ANOVA) followed by a *post hoc t*-test with the Bonferroni correction between techniques (rheology, indentation, NICR, VCCE). For the analysis, *p*-values < 0.05 were considered significant, where $p < 0.05$ is denoted with *, <0.01 with **, and <0.001 with ***. When possible, separate tests were conducted on white matter and gray matter regions of the same brain tissue. Macroscale rheology did not distinguish between white and gray matter regions (i.e., homogenized response inherent in technique for samples of this geometry), so those data were compared with either white or gray matter data obtained from the other three techniques. While the goal of this work was not to test differences between or among animals, we conducted ANOVA on averaged measurements for each animal (i.e., replicate experiments for tissue obtained from each animal was averaged) because only one value of E can be obtained from a series of NICR measurements on a given tissue slice.

3. Results

3.1 Measurement of porcine brain tissue apparent Young's modulus by rheology, indentation, NICR, and VCCE

To determine whether NICR and VCCE were viable characterization techniques for brain tissue, we compared their apparent Young's moduli to indentation and rheology under near "quasistatic" but finite deformation rates (i.e., deformation occurred on the order of 10s to 100s of seconds, but strain rates were difficult to define; see Methods). While these magnitudes do not represent a true "equilibrium" modulus, they allowed us to compare quantitatively these characterization methods and evaluate whether development of VCCE or NICR should be pursued further.

Figure 1 and Table 1 show the apparent Young's modulus of porcine brain measured by rheology, indentation, NICR and VCCE techniques. With rheology, which measures an averaged or homogenized modulus of the tissue, we measured an apparent Young's modulus E of 0.75 ± 0.06 kPa. With indentation, we measured E of 0.97 ± 0.40 kPa and 0.86 ± 0.20 kPa for white and gray matter, respectively. The magnitudes obtained from these two conventional techniques agreed with that reported by others (Budday et al., 2015; Budday et al., 2017; van Dommelen et al., 2010).

Similar to indentation, NICR and VCCE allow for localized measurements within either white or gray matter. Since surface tension affects the measured critical pressure in NICR, we measured this pressure for several needle radii to quantify surface tension $\gamma$and then calculate E from Eq. (**10**) for each sample. We thus obtained E of 4.8 ± 1.0 kPa and 3.7 ± 0.7 kPa for white and gray matter, respectively, which both significantly exceeded the magnitude we obtained via rheology and indentation. (Similarly, in murine brain, we found a Young's modulus of 0.7 ± 0.1 kPa, 1.5 ± 0.3 kPa and 3.9 ± 1.4 kPa for rheology, indentation and NICR, respectively; for indentation and NICR, these magnitudes are the arithmetic mean of data obtained on white and gray matter (Fig. S1).) In contrast to NICR, experiments using VCCE on porcine brain tissue indicated E of 0.92 ± 0.01 kPa and 0.76 ± 0.02 kPa for white and gray matter locations, respectively. Details on the characterization of the Ogden parameter α and the variability between measurements of different animals and location-based measurements is discussed in detail in Supplementary Materials S2. Significant differences were observed in each one-way ANOVA computed for white matter ($p < 0.001$) and for gray matter ($p < 0.001$). *Post hoc* comparisons showed significant differences between rheology and NICR ($p < 0.01$, ** and $p < 0.0001$, ###), indentation and NICR ($p < 0.01$, ** and $p < 0.0001$, ###),

ARTICLE

and VCCE and NICR ($p < 0.05$, * and $p < 0.001$, ##), for white and gray matter, respectively. No other significant differences were identified.

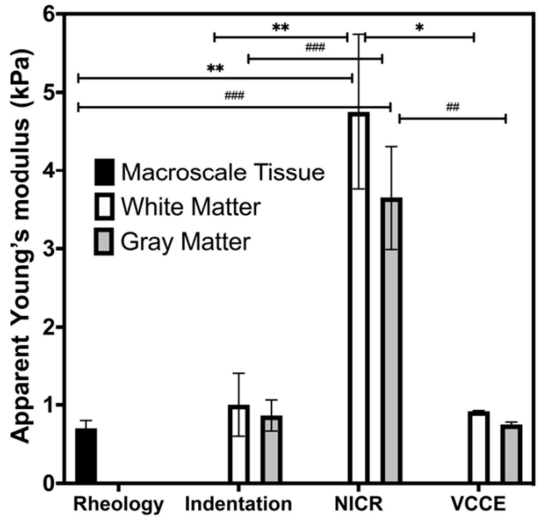

Figure 1: Apparent Young's modulus of porcine brain measured by rheology, instrumented indentation, NICR and VCCE. Data reflecting the homogenized or macroscale properties of brain tissue are accessible by rheology (black), whereas localized measurements are shown for indentation, NICR and VCCE for white matter (white) and gray matter (gray). The average apparent Young's modulus for NICR is significantly higher than that of rheology, indentation and NICR. There are no other significant differences between techniques. Error bars represent ± standard error of the mean. Data was analyzed using a one-way analysis of variance followed by a Bonferroni multiple comparison test with 95% confidence interval. *, ** for white matter indicate p <0.05, p < 0.01 and ## and ### for gray matter indicate p <0.001, and p <0.0001, respectively.

Table 1: Apparent Young's modulus of porcine brain (mean ± standard error of the mean).

	Rheology	**Indentation**		**NICR**		**VCCE**	
	-	White matter	Gray matter	White matter	Gray matter	White matter	Gray matter
E (kPa)	0.75 ± 0.06	0.97 ± 0.40	0.86 ± 0.20	4.8 ± 1.0	3.7 ± 0.7	0.92 ± 0.01	0.76 ± 0.02

3.2 Modeling predicts that cavitation instability is unlikely in strain-stiffening tissues

We used analytical and finite element models of cavity growth to simulate the pressure-stretch relationship in the absence of surface tension (Fig. 2a) and in the presence of surface tension (Fig. 2b) for the neo-Hookean and Ogden material models. The analytical model of a spherical cavity relates pressure P vs. circumferential stretch λ at the surface, while the FE model reports pressure vs. effective stretch λ_{eff}, consistent with the prior FE work of Hutchens and Crosby. The FE model has a geometry with the needle retracted from its initial position, as shown in Fig. 2c. From Fig. 2a, we observed that the FE model reported a similar relationship between P/E and stretch to the analytical model, and that the retracted needle geometry (of an initially cylindrical cavity Fig. 2c) showed a near-spherical geometry, at low stretches Fig. 2c(ii) (center) and especially at larger stretches (right). We note that in separate FE simulations reported in Supplementary Materials S4, we also repeated the same boundary conditions as assumed by Hutchens and Crosby (Hutchens and Crosby, 2014) and obtained similar results, but we reasoned those boundary conditions that prohibited slip between the needle and tissue less accurately approximated the experimental conditions. Those simulations did not agree with the spherical geometry analytical model, predicting substantially higher pressures than analytical results.

Since cavitation instabilities occur when there is either a plateau or maximum in the pressure-stretch curve, our FE and spherical geometry analytical models did not predict cavitation for a material well described as a 2-term Ogden model (the same constitutive law as adopted by Hutchens and Crosby (Hutchens and Crosby, 2014), due to appreciable strain stiffening. This result was guaranteed for the spherical geometry because the Ogden constants were not in the range for which there is a finite cavitation pressure (see Eq. (**9**)). Indeed, both the spherical and needle geometries with the Ogden material behavior showed a pressure-stretch curve that continues to increase with increasing stretch, unlike the neo-Hookean model for which P/E asymptotically approached 5/6 at increasing stretch (Fig. 2a). When the effect of surface tension between air and tissue was superimposed with elastic resistance to deformation, the surface tension provided a larger driving force for cavitation instability because stress decreases with increasing stretch for λ > 1.5. However, even when surface tension was incorporated into the model for magnitudes of Young's modulus and needle radius for which surface tension effect is more likely to dominate over the elastic response (e.g., low modulus $E \sim 1$ kPa and low needle radius $R \sim 100$ μm), there was no maximum observed in the pressure-stretch curve. Such a lack of maximum implies that cavitation is not expected under such

conditions due to strain stiffening of the (Ogden model) tissue. This is an important observation, in that the cavitation event was assumed rather than observed directly in our NICR experiments.

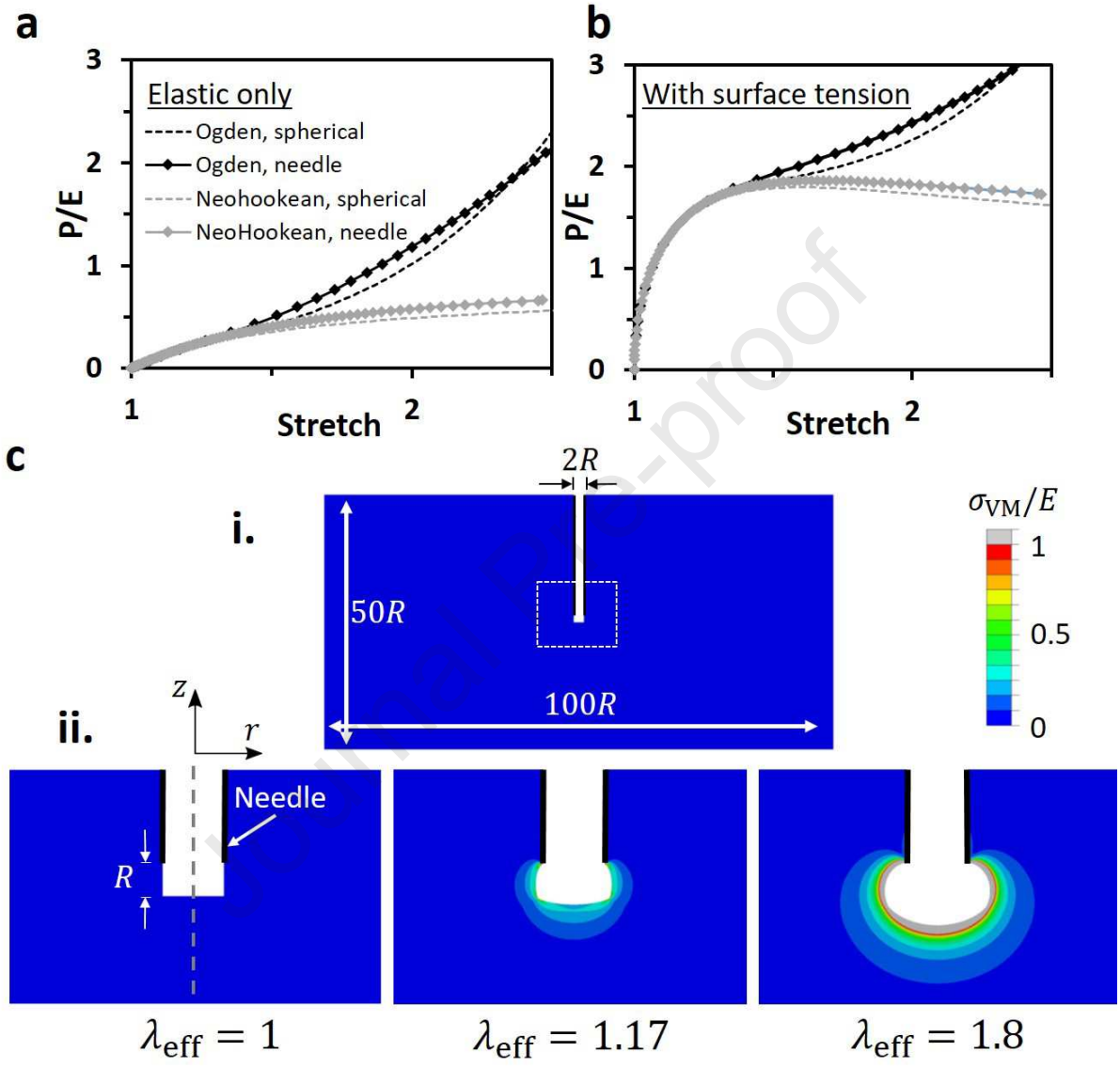

Figure 2. (**a**) Pressure-stretch responses, normalized by Young's modulus E for a neo-Hookean model (gray) and an Ogden model of brain tissue, used by Hutchens and Crosby (black) (Hutchens and Crosby, 2014), with $\alpha_1 = 4$, $\alpha_2 = 8$, $E_1 = E_2$. Dotted lines represent analytical results for a pressurized sphere, and circles represent finite element models of a cylindrical needle geometry. The neo-Hookean model approaches the asymptotic value $P/E = 5/6$, indicating expected cavitation, whereas the Ogden model shows extensive strain stiffening behavior without an asymptotic plateau, suggesting cavitation instabilities will not occur. (**b**) Pressure-stretch from (a) with surface tension included using a needle radius of 100 μm, surface tension of 72 mN/m, and Young's modulus of 1 kPa. A neo-Hookean material would cavitate under these conditions, as a clear peak pressure is observed. However, even with these conservative model values where the effect of surface tension is most pronounced (i.e., low needle radius, low Young's modulus), the strain stiffening behavior of the Ogden model does not allow for a maximum value in the pressure-stretch curve, and thus cavitation should not occur. (**c**) Axisymmetric finite element modeling of the needle geometry for the brain tissue shown in (a) with effective stretches of (left) $\lambda_{\text{eff}} = 1$, (middle) $\lambda_{\text{eff}} =$

ARTICLE

1.17, and (right) $\lambda_{\text{eff}} = 1.8$. Stresses are expressed as the von Mises stress normalized by the Young's modulus. The top panel represents the full geometry (with a needle outer radius R, a width of $100R$ and height of $50R$) and the bottom panel represents a zoom of the full geometry. In the undeformed configuration (i.), the initial unpressurized cylindrical void has a radius R and height R. As the void is pressurized, the deformation approaches a spherical geometry as stretch increases (ii.).

4. Discussion

Changes in the elastic properties of brain tissue have been correlated with progression of neurodegenerative disorders, traumatic brain injury, and brain cancers (Alfasi et al., 2013; Jamin et al., 2015; Murphy et al., 2011; Shafieian et al., 2009) Previous studies probing different components of the brain have identified that brain tissue exhibits location-dependent mechanical properties such as intraregional anisotropy for white matter in contrast to gray matter (Franceschini et al., 2006; Hrapko et al., 2008a; Prange and Margulies, 2002), interregional variations in different anatomical regions of the brain (Chen et al., 2015; Lee et al., 2014; van Dommelen et al., 2010), and regional inhomogeneity between corpus callosum, corona radiata, brain stem and gray matter structures (Elkin et al., 2011; Prange and Margulies, 2002). However, prior investigations conducted in brain tissue most commonly explored mechanical properties via rheology (Budday et al., 2017; Chatelin et al., 2010; Hrapko et al., 2006; Rashid et al., 2012) and indentation (Budday et al., 2015; Gefen and Margulies, 2004; Pogoda et al., 2014; van Dommelen et al., 2010). Both of those methods require or at least provide greater signal-to-noise ratio if the brain tissue is sectioned as slices that facilitate normal and uniform contact with the measurement instrument (plate or probe). Further, depending on the size of the brain (i.e., size of the animal) relative to the geometric details of the experiment (e.g., indentation probe diameter), those techniques can be limited in spatial resolution that can distinguish white and gray matter or anatomical regions.

Needle-induced cavitation rheology (NICR) and volume-controlled cavity expansion (VCCE) are two more recently developed techniques that provide spatial resolution on the order of 100 μm, and also do not require tissue sectioning if the tissue region of interest is accessible via needle penetration (Cui et al., 2011; Jansen et al., 2015; Kundu and Crosby, 2009; Zimberlin et al., 2010). NICR has recently been used to explore mechanical properties of polymers and tissues from the eye, bone marrow, lung and skin, highlighting its capabilities of testing local mechanical properties of compliant biological matter (Chin et al., 2013; Cui et al., 2011; Jansen et al., 2015; Polio et al., 2018). Similarly, VCCE incorporates the same methodology of NICR but controls cavity volume with an incompressible working fluid that is immiscible in the brain tissue (Raayai-Ardakani et al., 2019a; Raayai-Ardakani and Cohen, 2019). This is advantageous in tissues such as brain tissue for which the cavity volume and cavitation event cannot be visually observed due to the highly scattering optical properties of most tissues. Here we measured apparent modulusof porcine brain via NICR and VCCE, in comparison with rheology and indentation, to validate their applicability in obtaining E at a specific tissue location. We note again here that this measured modulus is not a true equilibrium elastic modulus due to potential contributions of viscoelastic and poroelastic effects. Moreover, the effective strain rates were not equivalent among techniques, and not easily defined for VCCE, NICR or indentation. Further, preconditioning of brain tissue has been reported to alter the measured tissue stiffness (Franceschini et al. 2006, Budday et al. 2017, Budday et al. 2019), and different experimental methods can also induce different strain histories (e.g., slight sample compression prior to data acquisition in shear rheology). Therefore, our reported magnitude of E should be considered within the context of the method limitations and underlying assumptions of material deformation. Nevertheless, each technique could be used to compare relative stiffness among tissue specimens analyzed by that technique for a given testing protocol (e.g., same effective strain rates). Similarly, our comparison of E among techniques should be viewed in the context of each approaches' limitations and assumptions. This comparison was a first validation step for VCCE and NICR in brain tissue characterization; modifications of the method and analysis to quantify rate-dependent constitutive properties are nontrivial and require additional considerations.

Our measurements of E by VCCE were in better agreement with conventional techniques than E determined by NICR. From our apparent Young's modulus comparison with conventional techniques shown in Fig. 1, we measured E of 0.75 + 0.06 kPa for rheology and E of 0.97 + 0.40 kPa and 0.86 + 0.20 kPa for white and gray matter, respectively, via instrumented indentation. These values are in reasonable agreement with those reported in work by others using similar experimental approaches (Budday et al., 2015; Chatelin et al., 2010; Franze et al., 2013; Hrapko et al., 2006). For example, (Budday et al., 2015) conducted instrumented indentation on porcine brain with a 1.5 mm

diameter flat punch geometry under 1 um/min-160 um/min displacement rates, and they reported apparent Young's moduli of 1.3-2.5 kPa and 0.69-1.4 kPa for white matter and gray matter, respectively. Using the same indenter geometry to characterize porcine brain, (Kaster et al., 2011) reported an apparent Young's modulus of 1.9 kPa and 1.2 kPa for white and gray matter, respectively, under near quasi-static oscillatory loading. Oscillatory shear rheology measurements reported by (Hrapko et al., 2006) for white matter (at frequency ranges of 0.04 to 16 Hz) resulted in a shear storage modulus ranging from 0.27 to 0.95 kPa. Our own determination of E using NICR were 4.8 ± 1.0 kPa and 3.7 ± 0.7 kPa for white and gray matter, respectively, which are more than threefold higher than the stiffness estimated from conventional techniques by us (for the same animal tissue sources and experimentalists). Our determination of E using VCCE, in contrast, was 0.92 ± 0.01 kPa and 0.76 ± 0.02 kPa for white and gray matter, respectively, and thus similar to that found via indentation and rheology. However, previous studies of other materials with NICR have shown agreement with shear rheology and indentation-based techniques, such as E measured for synthetic compliant polymers such as hydrogels (Kundu and Crosby, 2009; Zimberlin et al., 2007). In prior studies of biological tissues, some have reported a higher value via NICR in contrast to other techniques for tissues such as those obtained from bone marrow and lung (Jansen et al., 2015; Polio et al., 2018) while others have shown good agreement for tissues such as those from the eye lens (Cui et al., 2011). Hence, we next sought to understand why NICR analysis of brain tissue would yield a higher apparent Young's modulus in comparison to other approaches.

We begin with the assumptions specific to either VCCE or NICR analysis. In both approaches, we assume hyperelastic material behavior and formation of a spherical cavity upon sufficiently high pressure. The main difference is that, in NICR, the magnitude of the maximum pressure is used to calculate E, whereas in VCCE, the pressure-volume relationship preceding the maximum pressure point is fit to calculate E. In NICR, we specifically assume that the material behaves in a neo-Hookean manner (Eq. (**3**)), which leads to an elastic cavitation instability at sufficiently high pressure. Assuming the effect of surface tension is modeled from Eq. (**10**), we find E by extrapolating the critical pressure to an infinite needle radius (a hypothetical condition under which the surface tension contribution is assumed to be zero, as can be observed from Eq. (**4**)). In VCCE, we assume that a cavity of initially unknown volume and shape expands spherically under increasing pressure. With a sufficiently large needle radius (to minimize surface tension contributions), we can fit parameters from an assumed hyperelastic constitutive model to the increase in measured pressure as a function of controlled increase in incompressible fluid volume injected. In both approaches, we assume that the deformation rate is sufficiently slow such that viscoelastic effects of the material response are negligible, and that the material behaves hyperelastically. We emphasize that while the deformation mechanism is essentially the same in both techniques (except for the pressurizing fluid, which must be incompressible in VCCE and can be either incompressible or compressible in NICR), the main difference is the assumption of elastic cavitation at a singular critical pressure in NICR and the absence of that requirement in VCCE because the continuous pressure-volume data may be fit.

The discrepancy in the measurement of apparent Young's modulus by NICR compared with that obtained by rheology, indentation and VCCE is likely due to the assumption in NICR that the material behaves as a neo-Hookean solid. That constitutive law is inadequate to capture brain tissue deformation at large strains. While we cannot confirm this experimentally by direct imaging due to optical scattering of brain tissue, our computational analysis suggests that cavitation is unlikely in brain tissue due to strain stiffening under relevant conditions. From Fig. 2a, we see that an Ogden model of brain tissue reported previously (Franceschini et al., 2006) exhibits appreciable strain stiffening, and will not exhibit a maximum or plateau in the pressure-stretch curve; in contrast, the neo-Hookean material becomes increasingly compliant at higher stretch. Figure 2b suggests that, even with the conservative assumptions of low ratios of surface tension to Young's modulus γ/E and low needle radius (i.e., conditions where surface tension increases the driving force for cavitation due to a decreasing pressure-stretch relationship), the Ogden model of brain tissue does not predict cavitation. Thus, brain tissue's appreciable strain stiffening invalidates the underlying assumption (cavitation instability) in our analysis of NICR experimental data. Additionally, for materials or tissue as compliant as brain, the surface tension contribution relative to E in Eq. (10) can be large, and small errors can lead to high variability in the critical pressure vs. inverse needle radius relationship. Thus error of fitting P_c vs. $1/R$ experimental with Eq. (10) could lead to errors in measured modulus. As a result, E cannot be accurately measured from the critical pressure P_c from Eq. (**10**), and P_c may instead be indicative of fracture events within the tissue that may not be otherwise observable. This theoretical argument is also supported by our VCCE experiments, which show that the pressure-stretch response exhibited an increasing slope for stretch exceeding approximately 1.1, indicating that strain stiffening is exhibited over this range of stretch

ARTICLE

(Supplementary Materials section S4). Moreover, the fitted values for the Ogden parameter α were outside the range for a finite cavitation pressure for a spherical cavity (Supplementary Materials section S4). We note that the surface tension effect was assumed negligible in these experiments due to the relatively large needle radius,choice of working fluid and calibration procedure (Supplementary Materials section S2), which would imply that the response shown in Fig. 3c and Fig. S2 is governed predominantly by the elastic response of brain tissue. However, we could not confirm this assumption, as VCCE with smaller needle radii was not feasible due to friction artifacts in our system, and future work is necessary to clarify and quantify the surface tension effect fully. We hypothesize that damage or fracture governs the response at higher stretches. Thus, the cavitation assumption is likely invalid in NICR for strain stiffening materials such as brain tissue. It is noteworthy that we did not consider viscoelastic effects in our numerical analysis of cavity growth. Viscoelastic relaxation could provide a driving force for cavitation as stretch increases, which could potentially lead to a decrease in pressure with stretch resulting in a cavitation instability. However, the equations used to measure E from NICR assume elastic behavior. Since deformation rates are not easily measurable in opaque tissues such as brain, a cavitation event due (in part) to viscoelastic behavior would not lead to particularly useable information in measuring elastic properties. However, if the size of the cavity and the pressure could be concurrently measured, as they are in VCCE, this viscoelastic behavior could be characterized.

Next, we sought to evaluate validity of assumptions implicit in VCCE, given that the underlying equations were well fit to the pressure-volume data (or conversion to pressure-stretch data) but included assumptions of spherical cavity growth. Again, we cannot and did not observe the fluid-filled cavity shape directly due to light scattering within an opaque tissue, and so we must otherwise verify that the analytical solution is accurate because we use that relationship to calculate the hyperelastic parameters that define the brain tissue elastic properties. To verify the assumption of nearly spherical cavity geometry in VCCE, we conducted finite element modeling of the VCCE experiment, and we compared the pressure-stretch response from our analytic model to that of the finite element model. In our experiments, needles were retracted after insertion into the material, to relieve the induced residual stress and leaving a fluid-filled cavity in the original volume that was displaced by the needle. We replicated this condition in our model with an initially cylindrically shaped cavity. During pressurization, the cavity approached a spherical shape at relatively low circumferential stretch (λ_{eff} = 1.17) (Fig. 2c), and the pressure-stretch behavior was similar in magnitude and trend to the analytical solution (Fig. 2a). We note that prior finite element analyses by (Hutchens and Crosby, 2014) assumed different, and less likely, boundary conditions between the needle and tissue, and thus did not find these analytical models to be an accurate predictor of pressure-stretch simulations (see Supplemental Information S4).

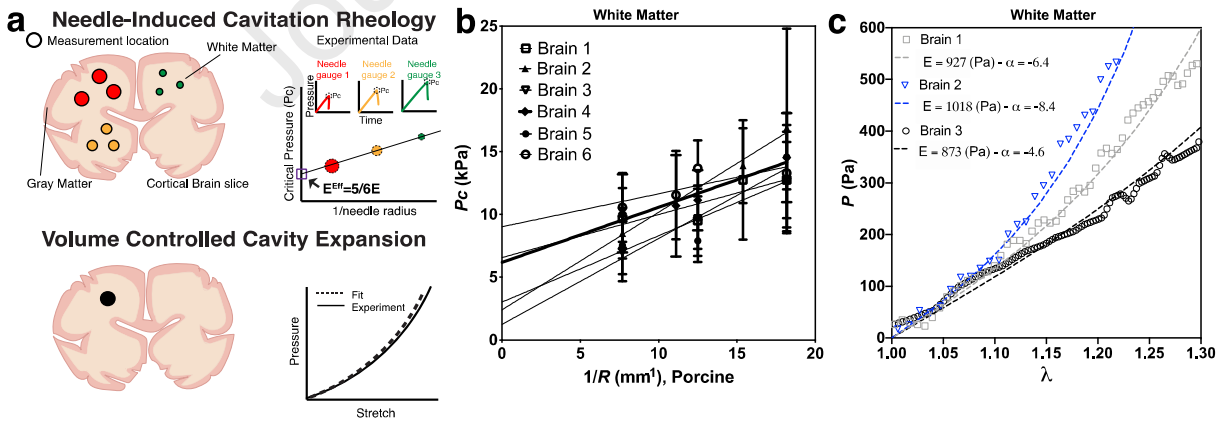

Figure 3. (**a**) Schematic of NICR and VCCE experimental setup. For NICR multiple measurements are taken with varying needle radii to measure the apparent Young's modulus while accounting for surface tension, E is related to the y-intercept of the fitted line. Individual P_c measurements are localized, but only a single average value for E is obtained per specimen. VCCE obtains a pressure-stretch response from a single localized measurement that is fitted to obtain E and a 1-term Ogden model that incorporates strain stiffening. (**b**) Critical pressure vs. inverse needle radius for porcine brain white matter measured by NICR. Variability in measurements at each needle radius may lead to large variation at the y-intercept (i.e., measured E). (**c**) VCCE experiment of brain white matter (symbols)

with a 1-term Ogden fit (dashed lines). Different colors represent different animal samples. Any hyperelastic model can be used in this approach, in principle.

The concurrent and continuous measurement of pressure and volume in VCCE, rather than only the determination of the critical pressure in NICR, provides more information about the constitutive behavior of the material used. If the value or importance of surface tension is unknown, NICR critical pressure must be measured at various needle radii (Fig. 3a), and E is calculated by extrapolating this curve to an infinite needle radius for which the effect of surface tension is negligible (Fig. 3b). Since critical pressure must be measured at various needle radii, it must also be tested at various locations in the material to obtain a single value of E for that sample. In contrast, VCCE allows measurement of E from a single pressurization in a single location (Fig. 3a) because the pressure can be measured as a function of volume and thus be fit to a hyperelastic constitutive model (Fig. 3c). Additionally, VCCE requires less stringent assumptions of the hyperelastic material behavior, and therefore can quantify a broader array of constitutive behavior than NICR. Although E can be determined for a given sample by only a single measurement via NICR (with an appropriate incompressible fluid and/or a sufficiently large needle), the lack of concurrent cavity volume measurement restricts the potential to fit the data to a constitutive model. VCCE can in theory be used to fit the material behavior to any isotropic, incompressible, hyperelastic model, such as the neo-Hookean model (Raayai-Ardakani et al., 2019a), the 1-term Ogden model used here, or other models as shown and compared in (Raayai-Ardakani et al., 2019a; Raayai-Ardakani and Cohen, 2019). Thus, for tissues like those of the brain, for which strain stiffening may prevent cavitation and for which neo-Hookean hyperelastic behavior is not observed under the relevant experimental conditions, VCCE could provide more accurate measurement of *E* than NICR. Further, VCCE allows for determination of E and α at each analyzed point in the tissue (Supplementary Materials section S2) and thus provides access to mapping spatial variation across a tissue (e.g., white vs. gray matter or cerebellum vs. cortex). Additionally, variability in these measurements could capture localized variation in tissue properties (e.g., vasculature), provided that such variation provided higher variability than experimental error. NICR provides similar mapping capability with the advantage of speed and ease of implementation. Additionally, measuring properties with critical pressure (by either NICR or VCCE), however, may provide more information about the potential failure or fracture events occurring in brain tissue, which is potentially very relevant for understanding damage incurred during traumatic injuries. Future work should address the meaning of the P_c value obtained with either NICR or VCCE for brain tissue.

While brain can exhibit appreciable viscoelastic behavior under a range of experimental conditions, the NICR and VCCE models assumed purely hyperelastic behavior due to relatively low deformation rates of the cavitation experiments. As shown by others, the brain's viscoelastic behavior typically follows a weak power law as a function of frequency (Chatelin et al., 2010). For measurements at high strain rates, such as in impact based techniques, brain tissue stiffness at short timescales is measured to be an order of magnitude higher than the relaxed tissue (Mijailovic et al., 2018). For stress relaxation or creep-based indentation techniques at lower strain rates with the longest relaxation timescale was measured to be on the order of 10 to 100 s (Gefen and Margulies, 2004), the stiffness at short time scales (< 1 s) was on the order of 1.5-2 times the equilibrium stiffness. This 10-100 s timescale overlaps with the timescale of deformation in the VCCE experiments (which were on the order of 10 s), and to a lesser extent with NICR (which were performed on the order of 100 s). Thus, the shorter experimental timescale of VCCE may overestimate the true equilibrium modulus of brain tissue. Indeed, studies have shown relaxation timescales longer than 100 s or 1000 s (Chatelin et al. 2010), suggesting that a true equilibrium modulus may not be attainable under what would be considered "quasistatic loading" under some practical operating conditions. Additionally, we did not consider poroelastic relaxation explicitly. Whether the capacity for poroelastic deformation of brain tissue actually contributes significantly in cavity expansion here depends – just as it depends in other contact mechanics contexts – on the relative length scales and time scales. These include loading time relative to characteristic fluid flow time, and radius of the needle-induced void and overall sample dimensions (Kalcioglu et al., 2012). We note that the cycling frequency of shear rheology was a choice replicating others' experimental choices for brain tissue (Jansen et al., 2015), but that reducing the frequency to ~0.01 Hz reduced the extracted apparent equilibrium modulus by only 15%. This reduction was similar to the confidence interval of moduli we extracted from 0.1 Hz data, and simply reflects the weak power law deformation of materials such as brain tissue. Loading rates and frequencies do affect magnitude of extracted parameters, but to a limited degree that can be difficult to distinguish from experimental variance for deformation times ranging seconds to minutes. At least for the current conditions in this study, however, the apparent Young's moduli determined from that method compared well with other methods that presumed linear elastic approximation. This study presents a first validation step in soft tissues for the VCCE

technique, which could be augmented to measure properties at higher strain rates and characterize nonlinear viscoelastic properties with improvements of the experimental setup.

A current difficulty in VCCE measurements is in the evaluation of the frictional forces of system, which currently limits the control of material deformation rates and thus quantification of viscoelastic behavior. The friction source is dominated by traction between the sealed piston and the syringe barrel, and can compete with the stiffness of samples as compliant as brain tissue or softer (apparent Young's modulus of less than about 1000 Pa). In the current experiments, we employed the same experimental procedure as discussed previously (Raayai-Ardakani et al., 2019a), and were able to subtract the frictional forces from the measurements. However, it would be of great interest to enhance the experimental setup by reducing the frictional forces in the system without removing the sealed nature of the piston and barrel of the syringes to ensure accurate volumetric readings. Such improvements in VCCE experimental setup could facilitate much higher strain rate loading, which in turn could allow for non-linear viscoelastic measurements. We note that NICR is not sensitive to these frictional forces, and can thus accommodate a broader range of needle sizes.

Here, we present and compare two approaches to probe local measurements of compliant, hydrated tissues: NICR and VCCE. These methods provide mechanical characterization at length scales finer that traditional techniques like rheology and instrumented indentation, and extend intentionally to hyperelastic deformation modes. We foresee the use of these approaches in characterizing additional biological materials – particularly "soft tissues" *in situ* and *ex vivo* – and the expansion of constitutive models beyond neo-Hookean to better describe strain stiffening and viscoelastic responses of biological tissues.

5.0 Conclusion

Elastic properties of mechanically compliant and hydrated biological tissues such as brain tissue are both challenging and important to measure accurately. Such data can be used to understand variations with disease, with species, or – at sufficiently high spatial resolution – with precise location information within a tissue or organ. Here we demonstrated that two versions of localized and fluid-pressurized cavitation can provide access to quantification of apparent Young's modulus in soft tissues including brain tissue, with a spatial resolution of 10s to 100s of micrometers. NICR provides a simple estimate of the apparent Young's modulus, as well as data related to the failure properties, across a large range of size scales and positions. However, quantitative agreement with more macroscale measurements of apparent Young's modulus for strain stiffening tissues, such as brain tissue, is limited chiefly because a cavitation instability is unlikely to occur in such tissues; therefore these NICR estimates of apparent Young's modulus may have been inaccurate. VCCE can be applied to strain stiffening tissues, and as we demonstrated can obtain multiple elastic constants for different hyperelastic constitutive models. Further, from our internal comparison of these approaches with more conventional microscale and macroscale approaches (instrumented indentation and shear rheology), VCCE returns apparent Young's moduli E for brain tissue that are in better agreement with those methods. This is attributable in large part to the acceptable assumptions of the VCCE approach for tissues, such as brain, that are strain stiffening (increasing internal stress with increasing applied strain). Additionally, VCCE is amenable to fitting different hyperelastic models that best describe the deformation of the specific tissue region of interest. In summary, these cavitation-based approaches offer access to mechanical properties of spatially complex and mechanically compliant hydrated tissues including that of the central nervous system, and the volume-controlled variant of this approach affords an accuracy and spatial resolution that is advantageous for detailed comparisons of biological conditions.

Acknowledgments

We are grateful to Michael Imburgia, Shruti Rattan, Katie Bittner, and Lauren Jansen for technical assistance and insightful conversations. We also acknowledged funding from the MIT Department of Materials Science & Engineering (A.S.M.), Michael & Sonja Koerner Professorship (K.J.V.V.). A.J.C. and S.R.P. acknowledge funding from the Office of Naval Research under grant ONR N000014-17-1-2056. S.G. acknowledge funding from a Northeast Alliance for the Graduate Education and Professoriate (NEAGEP) fellowship.

ARTICLE

References

Alfasi, A.M., Shulyakov, A.V., Del Bigio, M.R., 2013. Intracranial biomechanics following cortical contusion in live rats. Journal Neurosurgery 119, 1255-1262.

Boulet, T., Kelso, M.L., Othman, S.F., 2011. Microscopic magnetic resonance elastography of traumatic brain injury model. Journal of Neuroscience Methods 201, 296-306.

Budday, S., Nay, R., de Rooij, R., Steinmann, P., Wyrobek, T., Ovaert, T.C., Kuhl, E., 2015. Mechanical properties of gray and white matter brain tissue by indentation. Journal of the Mechanical Behavior of Biomedical Materials 46, 318-330.

Budday, S., Ovaert, T.C., Holzapfel, G.A., Steinmann, P., Kuhl, E., 2019. Fifty shades of brain: a review on the mechanical testing and modeling of brain tissue. Archives of Computational Methods in Engineering, 1-44.

Budday, S., Sommer, G., Haybaeck, J., Steinmann, P., Holzapfel, G.A., Kuhl, E., 2017. Rheological characterization of human brain tissue. Acta Biomaterialia 60, 315-329.

Canovic, E.P., Qing, B., Mijailovic, A.S., Jagielska, A., Whitfield, M.J., Kelly, E., Turner, D., Sahin, M., Van Vliet, K.J., 2016. Characterizing Multiscale Mechanical Properties of Brain Tissue Using Atomic Force Microscopy, Impact Indentation, and Rheometry. Journal of Visualized Experiments, e54201.

Chatelin, S., Constantinesco, A., Willinger, R., 2010. Fifty years of brain tissue mechanical testing: from in vitro to in vivo investigations. Biorheology 47, 255-276.

Chen, F., Zhou, J., Li, Y., Wang, Y., Li, L., Yue, H., 2015. Mechanical Properties of Porcine Brain Tissue in the Coronal Plane: Interregional Variations of the Corona Radiata. Annals of Biomedical Engineering 43, 2903-2910.

Cheng, S., Bilston, L.E., 2007. Unconfined compression of white matter. Journal of Biomechanics 40, 117-124.

Cheng, S., Clarke, E.C., Bilston, L.E., 2008. Rheological properties of the tissues of the central nervous system: a review. Medical Engineering Physics 30, 1318-1337.

Chin, M.S., Freniere, B.B., Fakhouri, S., Harris, J.E., Lalikos, J.F., Crosby, A.J., 2013. Cavitation rheology as a potential method for in vivo assessment of skin biomechanics. Plastic Reconstruction Surgery 131, 303e-305e.

Chou-Wang, M.S.O., Horgan, C.O., 1989. Void nucleation and growth for a class of incompressible nonlinearly elastic materials. International journal of solids and structures 25, 1239-1254.

Cui, J., Lee, C.H., Delbos, A., McManus, J.J., Crosby, A.J., 2011. Cavitation rheology of the eye lens. Soft Matter 7, 7827-7831.

Elkin, B.S., Ilankova, A., Morrison, I.I.I.B., 2011. Dynamic, Regional Mechanical Properties of the Porcine Brain: Indentation in the Coronal Plane. Journal of Biomechanical Engineering 133, 071009-071009-071007.

Elkin, B.S., Morrison, B., 2013. Viscoelastic properties of the P17 and adult rat brain from indentation in the coronal plane. Journal of Biomechanical Engineering 135, 114507.

Franceschini, G., Bigoni, D., Regitnig, P., Holzapfel, G.A., 2006. Brain tissue deforms similarly to filled elastomers and follows consolidation theory. Journal of the Mechanics and Physics of Solids 54, 2592-2620.

Franze, K., Janmey, P.A., Guck, J., 2013. Mechanics in neuronal development and repair. Annual Review of Biomedical Engineering 15, 227-251.

Gefen, A., Margulies, S.S., 2004. Are in vivo and in situ brain tissues mechanically similar? Journal of Biomechanics 37, 1339-1352.

Gent, A.N., 2005. Elastic instabilities in rubber. International journal of non-linear mechanics 40, 165-175.

Green, M.A., Bilston, L.E., Sinkus, R., 2008. In vivo brain viscoelastic properties measured by magnetic resonance elastography. NMR in Biomedicine: An International Journal Devoted to the Development and Application of Magnetic Resonance In vivo 21, 755-764.

Horgan, C.O., Polignone, D.A., 1995. Cavitation in nonlinearly elastic solids: A review. Applied Mechanics Reviews, 1995, 48, 471–485

Hrapko, M., van Dommelen, J.A., Peters, G.W., Wismans, J.S., 2006. The mechanical behaviour of brain tissue: large strain response and constitutive modelling. Biorheology 43, 623-636.

Hrapko, M., van Dommelen, J.A., Peters, G.W., Wismans, J.S., 2008a. Characterisation of the mechanical behaviour of brain tissue in compression and shear. Biorheology 45, 663-676.

Hrapko, M., van Dommelen, J.A., Peters, G.W., Wismans, J.S., 2008b. The influence of test conditions on characterization of the mechanical properties of brain tissue. Journal of Biomechanical Engineering 130, 031003.

Hutchens, S.B., Crosby, A.J., 2014. Soft-solid deformation mechanics at the tip of an embedded needle. Soft Matter 10, 3679-3684.

Hutchens, S.B., Fakhouri, S., Crosby, A.J., 2016. Elastic cavitation and fracture via injection. Soft Matter 12, 2557-2566.

Jagielska, A., Norman, A.L., Whyte, G., Vliet, K.J.V., Guck, J., Franklin, R.J.M., 2012. Mechanical environment modulates biological properties of oligodendrocyte progenitor cells. Stem cells and development 21, 2905-2914.

Jamin, Y., Boult, J.K.R., Li, J., Popov, S., Garteiser, P., Ulloa, J.L., Cummings, C., Box, G., Eccles, S.A., Jones, C., Waterton, J.C., Bamber, J.C., Sinkus, R., Robinson, S.P., 2015. Exploring the biomechanical properties of brain malignancies and their pathologic determinants in vivo with magnetic resonance elastography. Cancer Research 75, 1216-1224.

Jansen, L.E., Birch, N.P., Schiffman, J.D., Crosby, A.J., Peyton, S.R., 2015. Mechanics of intact bone marrow. Journal of the Mechanical Behavior of Biomedical Materials 50, 299-307.

Kalcioglu, Z.I., Mahmoodian, R., Hu, Y., Suo, Z., Van Vliet, K.J., 2012. From macro- to microscale poroelastic characterization of polymeric hydrogels via indentation. Soft Matter 8, 3393–3398.

Kaster, T., Sack, I., Samani, A., 2011. Measurement of the hyperelastic properties of ex vivo brain tissue slices. Journal of biomechanics 44, 1158-1163.

Kundu, S., Crosby, A.J., 2009. Cavitation and fracture behavior of polyacrylamide hydrogels. Soft Matter 5, 3963-3968.

Lee, S.J., King, M.A., Sun, J., Xie, H.K., Subhash, G., Sarntinoranont, M., 2014. Measurement of viscoelastic properties in multiple anatomical regions of acute rat brain tissue slices. Journal of the Mechanical Behavior of Biomedical Materials 29, 213-224.

Mihai, L.A., Chin, L.K., Janmey, P.A., Goriely, A., 2015. A comparison of hyperelastic constitutive models applicable to brain and fat tissues. J. R. Soc. Interface. 12(110), 20150486.

Mihai, L.A., Budday, S., Holzapfel, G.A., Kuhl, E., Goriely, A., 2017. A family of hyperelastic models for human brain tissue. Journal of the Mechanics and Physics of Solids 106, 60-79.

Mijailovic, A.S., Qing, B., Fortunato, D., Van Vliet, K.J., 2018. Characterizing viscoelastic mechanical properties of highly compliant polymers and biological tissues using impact indentation. Acta Biomaterialia 71, 388-397.

Miller, K., Chinzei, K., 2002. Mechanical properties of brain tissue in tension. J Biomech 35, 483-490.

Miller, K., Chinzei, K., Orssengo, G., Bednarz, P., 2000. Mechanical properties of brain tissue in-vivo: experiment and computer simulation. Journal of Biomechanics 33, 1369-1376.

Murphy, M.C., Huston, J., 3rd, Jack, C.R., Jr., Glaser, K.J., Manduca, A., Felmlee, J.P., Ehman, R.L., 2011. Decreased brain stiffness in Alzheimer's disease determined by magnetic resonance elastography. Journal Magnetic Resonance Imaging 34, 494-498.

Nicolle, S., Lounis, M., Willinger, R., 2004. Shear properties of brain tissue over a frequency range relevant for automotive impact situations: new experimental results. SAE Technical Paper.

Nicolle, S., Lounis, M., Willinger, R., Palierne, J.F., 2005. Shear linear behavior of brain tissue over a large frequency range. Biorheology 42, 209-223.

Pogoda, K., Chin, L., Georges, P.C., Byfield, F.J., Bucki, R., Kim, R., Weaver, M., Wells, R.G., Marcinkiewicz, C., Janmey, P.A., 2014. Compression stiffening of brain and its effect on mechanosensing by glioma cells. New Journal of Physics 16, 075002.

Polio, S.R., Kundu, A.N., Dougan, C.E., Birch, N.P., Aurian-Blajeni, D.E., Schiffman, J.D., Crosby, A.J., Peyton, S.R., 2018. Cross-platform mechanical characterization of lung tissue. PloS one 13, e0204765.

Prange, M.T., Margulies, S.S., 2002. Regional, directional, and age-dependent properties of the brain undergoing large deformation. Journal of Biomechanical Engineering 124, 244-252.

Prevost, T.P., Balakrishnan, A., Suresh, S., Socrate, S., 2011. Biomechanics of brain tissue. Acta Biomaterialia 7, 83-95.

Raayai-Ardakani, S., Chen, Z., Earl, D.R., Cohen, T., 2019a. Volume-controlled cavity expansion for probing of local elastic properties in soft materials. Soft matter 15, 381-392.

ARTICLE

Raayai-Ardakani, S., Cohen, T., 2019. Capturing strain stiffening using Volume Controlled Cavity Expansion. Extreme Mechanics Letters 31, 100536.

Raayai-Ardakani, S., Earl, D.R., Cohen, T., 2019b. The intimate relationship between cavitation and fracture. Soft matter 15, 4999-5005.

Rashid, B., Destrade, M., Gilchrist, M.D., 2012. Mechanical characterization of brain tissue in compression at dynamic strain rates. Journal of the Mechanical Behavior of Biomedical Materials 10, 23-38.

Shafieian, M., Darvish, K.K., Stone, J.R., 2009. Changes to the viscoelastic properties of brain tissue after traumatic axonal injury. Journal Biomechanics 42, 2136-2142.

Shull, K.R., Ahn, D., Chen, W.L., Flanigan, C.M., Crosby, A.J., 1998. Axisymmetric adhesion tests of soft materials. Macromolecular Chemistry and Physics 199, 489-511.

Streitberger, K.J., Wiener, E., Hoffmann, J., Freimann, F.B., Klatt, D., Braun, J., Lin, K., McLaughlin, J., Sprung, C., Klingebiel, R., Sack, I., 2011. In vivo viscoelastic properties of the brain in normal pressure hydrocephalus. NMR in Biomedicine 24, 385-392.

Tyler, W.J., 2012. The mechanobiology of brain function. Nature Reviews Neuroscience 13, 867-878.

Urbanski, M.M., Brendel, M.B., Melendez-Vasquez, C.V., 2019. Acute and chronic demyelinated CNS lesions exhibit opposite elastic properties. Scientific reports 9, 999.

van Dommelen, J.A., van der Sande, T.P., Hrapko, M., Peters, G.W., 2010. Mechanical properties of brain tissue by indentation: interregional variation. Journal of the Mechanical Behavior of Biomedical Materials 3, 158-166.

Velardi, F., Fraternali, F., Angelillo, M., 2006. Anisotropic constitutive equations and experimental tensile behavior of brain tissue. Biomechanics and Modelling in Mechanobiology 5, 53-61.

Wang, C., Tong, X., Yang, F., 2014. Bioengineered 3D brain tumor model to elucidate the effects of matrix stiffness on glioblastoma cell behavior using PEG-based hydrogels. Molecular Pharmaceutics 11, 2115-2125.

Wuerfel, J., Paul, F., Beierbach, B., Hamhaber, U., Klatt, D., Papazoglou, S., Zipp, F., Martus, P., Braun, J., Sack, I., 2010. MR-elastography reveals degradation of tissue integrity in multiple sclerosis. Neuroimage 49, 2520-2525.

Zimberlin, J.A., McManus, J.J., Crosby, A.J., 2010. Cavitation rheology of the vitreous: mechanical properties of biological tissue. Soft Matter 6, 3632-3635.

Zimberlin, J.A., Sanabria-DeLong, N., Tew, G.N., Crosby, A.J., 2007. Cavitation rheology for soft materials. Soft Matter 3, 763-767.

Highlights

- Needle induced cavitation rheology (NICR) and volume-controlled cavity expansion (VCCE) are facile methods to measure the local Young's modulus *E* of brain tissue
- Elastic modulus for white and gray matter is estimated more accurately with VCCE, in part because of the assumptions governing data interpretation
- VCCE is a more accurate representation of the brain tissue constitutive response at elevated strains

Declaration of interests

☒ The authors declare that they have no known competing financial interests or personal relationships that could have appeared to influence the work reported in this paper.

☐The authors declare the following financial interests/personal relationships which may be considered as potential competing interests: